In vitro biofabrication of silver nanoparticles: Optimization, characterization, and activity against beta-lactamases-resistant *Enterococcus faecalis*

Bikhal Fattah
University of Sulaimani
Huner Arif
University of Sulaimani
Haider Hamzah (haider.hamzah@univsul.edu.iq)
University of Sulaimani https://orcid.org/0000-0003-4297-3647

Research Article

Keywords: Silver nanoparticles, Comamonas aquatica, Fusarium solani, Enterococcus faecalis

Posted Date: May 26th, 2021

DOI: https://doi.org/10.21203/rs.3.rs-557864/v1

Abstract

The rate at which nosocomial infections have spread throughout the globe has been alarming. Therefore, the data presented here sheds light on some aspects of AgNPs as promising anti-infective therapy. However, knowledge on the safe usage of AgNPs in the field of medicine is necessary to investigate. AgNPs synthesis, optimization, characterization, and mode of action against *Enterococcus faecalis* have been studied in this paper. We propose a combination of cell-free supernatant (C-FS) of the intimate organisms; *Fusarium solani* and *Comamonas aquatica* as synthesis catalysts. The optimization findings were at pH 9.0 for 72 h in 1 mM $AgNO_3$ using 1:2 v/v (C-FS : $AgNO_3$). UV-vis absorption peak appeared at 425 nm and the crystalline nature of synthesized particles was verified by XRD. FTIR analysis confirmed the presence of protein molecules that acted as reducing and stabilizing agents. Energy-dispersive X-ray analysis exhibited an intense peak at 3 KeV, confirming the formation of AgNPs. Further, FE-SEM images prove AgNPs synthesis. TEM and AFM analysis demonstrated that fabricated AgNPs were relatively monodispersed, approximately spherical, and of size 2-7.5 nm. The growth and biofilm of nosocomial *E. faecalis* were significantly decreased by the action of AgNPs. Furthermore, antibiotic resistance genes, bla_{TEM}, and bla_{CTX}, were detected in *E. faecalis*; both genes were degraded enormously via 9 % AgNPs. This is the first study proposing alternative sources to form AgNPs via synergistic metabolites of *F. solani* and *C. aquatica*. The results here offer a foundation for developing an effective therapy using AgNPs against nosocomial pathogens.

Introduction

In the last decade, the rate of antibiotic resistance has considerably elevated as pathogens evolve a variety of mechanisms for the resistance of antibiotics (Blair et al. 2015). As a phenomenon, antibiotic resistance is often associated with infection and is therefore also related to virulence, as in the cases of biofilm-producing bacteria (Patel 2005). Biofilm-producing bacteria are the cause of several acute and chronic human infections, such as the native valve endocarditis, pneumonia in cystic fibrosis patients, infection of chronic wounds and chronic otitis media, catheter associated infections and chronic bacterial prostatitis (Azevedo et al. 2017; Vestby et al. 2020). Most of the currently used antibiotics are becoming inefficient against the biofilm-associated multidrug-resistant microorganisms. Therefore, it has become necessary to search for alternative solutions to mitigate biofilm associated bacteria (Natan and Banin 2017). *Enterococcus faecalis* is one of the most common primary infectious enterococcal species identified in hospital-acquired infections (Dale et al. 2015). *E. faecalis* is a gram-positive bacterium found in humans as intestinal microflora; however, it is ranking among the most common nosocomial pathogens isolated from the bloodstream, surgical sites, and urinary tract infections (Fiore et al. 2019). It is also involved in clinical pathogensis such as wound infections, infective endocarditis, meningitis, uninray tract infection and even endodontic infections (Anderson et al. 2016). The virulence of *E. faecalis* is related to the ability to produce a biofilm composed mainly of specific cell surface protein (Esp), where the film plays a vital role in the adherence mechanism to surfaces, especially of medical devices in chronicly infected patients leading to nosocomial infections (Tendolkar et al. 2004). *E. faecalis* has the

propensity to acquire resistance determinants via horizontal gene transfer, and it has shown the frequent occurrence of antimicrobial resistance, especially to tetracycline and erythromycin (Woźniak-Biel et al. 2019).

Over the last years, less-than-100-nm nanoparticles have been receiving enormous attention due to their unique size-dependent electrical, optical, physical, and chemical properties (Saeb et al. 2014). Specifically, silver nanoparticles (AgNPs) possess a broad-spectrum of highly efficient antimicrobial, anticancer, anticoagulant, anti-inflammatory and antibiofilm activities (Xu et al. 2020). Other biological activities of AgNPs have also been explored, including wound repair (Gunasekaran et al. 2011) and promoting bone healing (Asgary et al. 2016), which make them an ideal candidate in medical and biological platforms. AgNPs exhibit less toxicity towards humans at lower concentrations; it has been widely incorporated in drugs under various forms such as salts, immobilized ions, or as nanoparticles (Le Ouay and Stellacci 2015). The exact mechanism of AgNPs against pathogenic bacteria is still not clear, however, there are various proposed mechanisms of action including disturbance of the cell membrane, alteration of cellular DNA and proteins, respiratory chain blockage by enzyme binding, or the generation of reactive oxygen species (ROS), which lead to cell death (Singh et al. 2018). Fabrication of stable and robust AgNPs is a very challenging task; physical methods have low yields, while the chemical ones cause harmful effects on the environment due to use of toxic solvents and the regeneration of hazardous by-products which can limit the use of AgNPs for clinical application (Zhang et al. 2016). Filamentous fungi have advantages over other microorganisms for biogenic synthesis of nanoparticles; they tolerate high concentrations of metals and secrete large amounts of metabolites that contribute to the stability of the nanoparticles (Netala et al. 2016). Qurbani and Hamzah (2020), have confirmed that the filamentous fungus *Fusarium solani* and gram-negative *Comamonas aquatica* grow well in co-culture and tolerate high concentrations of metals; the study reveals synergistic relationships between *C. aquatica* and *F. solani* that robustly remove metals in the culture medium. Here, we examined how the supernatants of *F. solani* and *C. aquatica*, collectively, can be used to synthesize AgNPs in vitro. The effect of AgNPs against a commonly local isolate of infection-derived *Enterococcus faecalis* was also studied.

Materials And Methods

Source of microorganisms

C. aquatica KQ_HH19 and *F. solani* KQ_HH19 were previously isolated and identified by (Qurbani and Hamzah 2020). For the purpose of the antimicrobial experiment, Gram positive *E. faecalis* was selected as a model. *E. faecalis* is a clinical bacterium isolated from a urine sample in Sulaymaniyah Teaching Hospitals. *E. faecalis* was identified via VITEK2 (BioMerieux, USA) instrument using a Gram-positive VITEK2 ID card.

Preparation of AgNPs using cell-free supernatant (C-FS)

C. aquatica and *F. solani* were used for synthesis of AgNPs. Fresh cultures of *C. aquatica* and *F. solani* were grown separately in a 250 mL Erlenmeyer flask that contained 100 mL of nutrient broth. Both

organisms were incubated at 30°C, in which the bacterial flask was incubated for 48 h, whereas the fungus remained for 72 h. The supernatants of the cultures were collected by centrifuging (Biofuge Stratose, Germany) at 5,000 rpm for 20 min at 4°C in sterile tubes and used for the synthesis of AgNPs. Three Erlenmeyer flasks were prepared; the first containing $AgNO_3$ solutions (Sigma, USA, purity 99.9%) without the supernatant as control, the second containing only the supernatant also as control and the third containing equal amounts of the supernatants of the bacterium and fungus. The latter was mixed with 1 mM of filter-sterilized $AgNO_3$ solution as a final concentration. Reaction mixtures were incubated for 72 h at room temperature under static conditions. The extracellular synthesis of AgNPs was monitored by visual inspection of the flasks for a change in color. The AgNPs were collected by high-speed centrifugation at 14,000 rpm for 20 min at 4°C using a cold centrifuge (Mikro 200R, UK). Supernatants were discarded and pellets of AgNPs were washed three times with autoclaved distilled water to remove the unconverted metal ions or any other constituents. The obtained precipitation was kept in Petri dishes and left in the oven for drying at about 40°C for 24 h (WTC Binder, Germany). The dried AgNPs were scraped out and obtained in powder form for further study (Hamedi et al. 2014; Rudakiya and Pawar 2017).

Optimization of bio-AgNPs

The effects of four variables on the product yield of AgNPs were optimized by varying one parameter at a time, including $AgNO_3$ concentration (0.5, 0.75 and 1.0 mM), pH values (5.0, 7.0, 9.0, and 11.0), reduction time (24, 48, and 72 h) and volume ratio (1:1, 1:2, 2:1 v/v C-FS: $AgNO_3$). All experiments were carried out in triplicates.

Characterization of AgNPs

UV–visible spectral analysis

The bio-reduction of Ag^+ ions was monitored with UV-visible spectrum and was recorded with UV-vis spectrophotometer (Kary60, USA) with a resolution of 2 nm within a range of A_{300} to A_{800} nm (Singh et al. 2018).

Fourier transform infrared (FTIR) spectroscopy

FTIR analysis of the dried powder of AgNPs was carried out by scanning the spectrum in the range of 400–4,000 cm^{-1} at a resolution of 4 cm−1 (PerkinElmer 1600, USA). FTIR measurements were applied to identify the possible biomolecules which are responsible for the reduction of silver ions to NPs and stabilization of AgNPs in colloidal solution (Birla et al. 2013).

X-ray diffraction analysis (XRD)

Crystal structure and size of the prepared AgNPs were investigated by X-ray diffraction technique, using an X 'Pert Pro diffractometer (Pan Analytical, Netherlands) equipped with Cu-K-α radiation (1.5406 Å), at

fixed operating voltage and current of 45 kV and 40 mA, respectively. The XRD glancing angles were arranged in the range of 10° ≤ 2θ ≤70°. The sample was dried and obtained in powder form as mentioned previously (Shahzad et al. 2019). The size of the nanoparticles was calculated using the Debye-Scherrer equation (Chand et al. 2019).

Field emission scanning electron (FE-SEM) and energy dispersive X-ray (EDX)

Morphological characteristics of AgNPs were further characterized via field emission scanning electron microscopy (Quanta 450, Netherlands). The sample for SEM was prepared by placing a drop of AgNPs solution on a gold-coated copper grid, dried at room temperature and transferred for analysis. SEM images were captured at 8448X magnification. Elemental composition of the synthesized nanoparticles was analyzed by energy dispersive X-ray spectroscopy (Bruker, Germany) implemented in SEM at 20 kV (Hamedi et al. 2014).

Transmission Electron Microscopy (TEM)

The shape and size of the AgNPs were determined by TEM (PHILIPS model CM120, Netherlands) operated at an accelerating voltage of 100 Kv. The sample for TEM analysis was prepared by dispersing the samples in distilled water through sonication for 15 min. After that, a drop of AgNPs were poured on the carbon-coated copper grids then left for drying at room temperature. A particle size distribution histogram was obtained by using a nano measuring software (Chand et al. 2019).

Atomic force microscopy (AFM)

The surface topography and morphology of AgNPs was studied by atomic force microscopy. A thin layer of the sample was prepared by dropping 100 μL of the sample on a glass slide and allowed to dry for 5 min. The slides were then scanned with AFM (BRUKER, ICON Instruments, USA). The AFM images were then taken with silicon cantilevers in contact mode. The AFM images were processed using ICON data processing software (Shahzad et al. 2019).

Action of AgNPs against *E. faecalis*

Agar well diffusion assay

Agar well diffusion assay was conducted to analyze the antimicrobial activity of AgNPs. In brief, *E. faecalis* was grown over night in LB broth at 37°C. The number of cells per milliliter was adjusted to be 10^8 CFU/mL, equivalent to 0.5 McFarland. Then, 100 µL culture broth was spread evenly on a Müeller-Hinton agar plates. Wells were made using gel puncture and 100 µL of different concentrations of AgNPs (12.5, 25, 50, 75, and 100 %) were loaded into certain wells. Also, 100 µL of LB broth was used as a control. The plates were incubated at 37°C for 24 h and the zone of inhibition was measured (mm). The assay was done in triplets (Ahmed et al. 2018).

Minimum inhibitory concentration assay (MIC)

To measure the MIC of AgNPs, fresh overnight culture of pathogenic *E. faecalis* isolate was adjusted to be 10^8 CFU/mL as mentioned previously. A bacterial culture of 120 µL was dispensed in 96-wells of sterile polystyrene microtiter plates and then 80 µL of an appropriate concentration of AgNPs (3, 6, 9, 12.5, 25, 50, 75, and 100 %) was added. LB broth (200 µL) was used as a negative control and 120 µL of bacterial culture mixed with 80 µL LB broth was applied as a positive control. The microdilution trays were incubated at 37°C overnight under a gentle shaking in the microplate incubator-shaker PST-60 HL Plus (BOECO, Germany). The absorbance of each well was measured at 600 nm using a microtiter ELISA reader (Biotech µQuant, USA). In addition, 5 µL was taken from each well and spotted onto LB agar plates, with all plates incubated at 37°C for 18 h. Growth percentage was calculated based on the average and standard deviation of triplicate results (Hamzah et al. 2018).

Biofilm inhibition assay

The biofilm degrading activity of AgNPs was determined by colorimetric method against *E. faecalis* according to (Hamzah et al. 2018) with a few modifications. A culture of *E. faecalis* was grown in LB broth for 24 h at 37°C. A Tissue Culture Plate (TCP) approach was used. 120 µL of bacteria culture (10^8 CFU/mL) were placed in a 96-well microtiter plate, with 80 µL of different concentrations of AgNPs (3, 6, 9, 12.5, 25, 50, 75, and 100%) added. In addition, 200 µL of LB broth was used as a negative control. The plate was then incubated for 24 h at 37°C under gentle shaking in microplate incubator-shaker PST60 HL Plus (BOECO, Germany). Biofilm was measured by discarding the medium and rinsing the wells three times with 200 µL phosphate buffer saline (PBS, pH 7.2). After drying, the attached cells were stained with crystal violet (0.1%) for 30 min. After staining, the liquid was discarded and the wells were washed three times with distilled water. The plate was then allowed to dry at room temperature, after which 200 µL ethanol (95%) was added to the wells to solubilize the stain. Then, the wells were read at 595 nm via Microplate Spectrophotometer (Biotech µQuant, USA). Optical density (OD) readings were used as an indicator of the bacterial biofilm formation then converted to percent of inhibition (%). Simultaneously, 5 µL was taken from each well and spotted on LB agar and Congo Red Agar (CRA) plates, followed by incubation at 37°C overnight. Briefly, CRA was prepared as followed: brain heart infusion (BHI, 37 g/L), sucrose (50 g/L), and agar (10 g/L) were prepared and autoclaved at 121°C for 15 min. Congo red dye (Sigma-Aldrich, Germany) (0.8 g/L) was also prepared simultaneously and added to warm (50°C) BHI agar. The color and texture of the colonies were then analyzed to evaluate biofilm efficacy (Hamzah et al. 2018). This experiment was conducted in triplets with averages and standard deviations (STDEV) calculated using Microsoft Excel.

Protein Leakage Assay

The effect of AgNPs on membrane damage of the cell was further studied by quantifying the leaked cytoplasmic proteins. Protein leakage from *E. faecalis* cells was determined by the A280 assay (Miksusanti et al. 2008) using NanoDrop 2000 (ThermoFisher, USA). Briefly, bacterial cell suspension with an absorbance of 0.2 at 600 nm (10^8 CFU/mL) was prepared in LB and treated with AgNPs at 0% and 9%

(v/v) for about 18 h. Samples were centrifuged at 14,000 rpm at 4°C for 5 min using Mikro 200R centrifuge (Hettich, UK). Afterwards, the collected supernatants were subjected for protein quantification.

Detection of *bla*$_{TEM}$ and *bla*$_{CTX}$ antibiotic resistance genes in *E. faecalis*

The polymerase chain reaction (PCR) method was performed to detect two antibiotic resistant genes, *bla*$_{CTX}$ and *bla*$_{TEM}$, in *E. faecalis*. Total genomic DNA from untreated and treated cells (the cells were treated with 9% AgNPs) was extracted using Presto™ Mini gDNA Bacteria Kit (Geneaid, Italy) following the manufacture's guidelines. PCR was performed via ThermoCycler T100^{TM} (Bio-Rad, Singapore). Novel primers were designed based on data from plasmids resistance genes collected from the NCBI nucleotide database (https://www.ncbi.nlm.nih.gov/nuccore). Specific primers were designed based on the multiple sequence alignment of *bla*$_{CTX}$ and *bla*$_{TEM}$ genes using Clustal Omega. The sequences of the selected primers are shown in Table 1. PCR reaction mixture set-up contained 10 µL master mix, 1 µL of forward and reverse primers each, 1 µL of DNA, and 7 µL of distilled water giving a total of 20 µL. The PCR protocol for 30 cycles was as follows: an initial denaturation at 94°C for 2 min, then 94°C for 30 sec, 55°C for 30 sec, 68°C for another 30 sec, followed by a final extension at 68°C for 7 min. The PCR products were analyzed by electrophoresis in a 1% agarose gel in TAE buffer at 90V for about 40 min, stained with ethidium bromide, and the image captured via MultiDoc-It™ Imaging System (UVP, USA).

Table 1 Primer sequences for detection of *bla*$_{CTX}$ and *bla*$_{TEM}$

*In the following primers, F denotes forward and R denotes reverse.

Statistical analysis

Microsoft Excel (Microsoft 2016) was used for all the statistical computations. Three independent measurements of each assay in this paper were pooled and subjected to statistical analysis.

Results

AgNPs optimization and characterization

In this paper, we found that the combination of *F. solani* KQ_HH19 and *C. aquatica* KQ_HH19 supernatants have the ability to reduce silver salt into silver nanoparticles substantially. Initially, the extracellular biogenic synthesis of AgNPs was confirmed throughout the visual color change in the reaction mixture as well as via UV–vis spectroscopy (Figure S1). The color change started after about 25 min of mixing the C-FS with $AgNO_3$ solution. Gradually, the intensity of the reaction mixture changed from pale yellow to dark brown after about 18 h of incubation due to the reduction of Ag^+ forming the AgNPs. The result here represents the broad and strong surface plasmon resonance peak (SPR) that evolved at 425 nm; it is a representative characteristic of AgNPs emergence. In the current study, optimal formation of AgNPs was studied to achieve, primarily, good monodispersity, stability, better yield, and biocompatibility of the particles at 25°C under light conditions; the reduction of silver ions was less at

dark conditions. Variation in reaction conditions such as $AgNO_3$ concentrations (Figure S2), pH values (Figure S3), the volume ratios of C-FS with $AgNO_3$ solution (Figure S4), and reduction times (Figure S5) directly affecting the productivity as noticed during the biogenic process. The intensity of UV-vis absorption spectra was optimized. The best conditions for AgNPs fabrication (Figure 1) were at pH 9.0 for 72 h in 1 mM of $AgNO_3$ using 1:2 v/v (C-FS : $AgNO_3$). Again, the SPR of silver occurs at 425 nm as depicted in Figure 1.

Figure 1. UV–visible spectrum of optimal conditions of AgNPs production. **Inset**: **A.** $AgNO_3$ solution without supernatant. **B.** C-FS. **C.** C-FS and $AgNO_3$ solution.

FTIR measurement of the dried sample was carried out to identify the possible interactions between metal and biomolecules surrounding the nanoparticles, which may have played a vital role in the reduction and stabilization of AgNPs (Figure 2A). The figure represents the spectrum that revealed the presence of eight distinct peaks at 1056, 1409, 1462, 1597, 1643, 2987, 3086 and 3279 cm^{-1} in the region of 400-4000cm^{-1}. The peaks at 3279 cm^{-1}, 3086 cm^{-1} and 2987cm^{-1} indicate the presence of alcohol O-H_{str}, primary amine N-H_{str}, and alkaine C-H_{str} vibration of protein respectively. The appearance of peaks at 1643 cm^{-1} and 1597cm-1 are of significant importance; recognizing C=O carbonyl group which is assigned to amide of protein. The other bands lie at 1462cm^{-1}, 1409cm^{-1}, and 1056 cm^{-1} which is a characteristic of aliphatic and aromatic organic compound that contain C-N_{str} vibration.

The crystalline structure of the AgNPs was investigated by XRD technique. The XRD pattern (Figure 2B) shows five characteristic peaks at 2θ values of about 27.84°, 32.25°, 46.26, 54.85° and 57.52°, which can be assigned the planes of (111), (200), (220), (311), and (222), respectively. All these reflection planes are matched to the face centered cubic (fcc) phase of crystalline silver Ag°The average estimated particle size of our sample was 16.46 nm obtained from the full width at half maximum (FWHM) of the peak corresponding to 200 planes by using Debye-Scherrer equation. FE-SEM was applied to determine the formation of silver nanoparticles. After drying, the thin layer was analyzed and pictured. The FE-SEM shows a presence of high-density of AgNPs with aggregations (Figure S6). The prepared nano-powder was also examined through energy dispersive X-ray analysis (EDX) for compositional analysis as shown in Figure S6. The EDX spectra of AgNPs displayed an optical absorption peak at 3 KeV, which is the characteristic peak for metallic AgNPs. The elemental mapping results of the biosynthesized nanoparticles indicate the maximum distribution of silver elements suggesting that the silver is the predominant element in the respective nanoproducts (Figure S6).

The data obtained from TEM images show that AgNPs have a mostly spherical in shape, the 3-5 nm in size and relatively monodispersed, with few agglomerated particles (Figure 2C). The particle size distribution curve shows that the range of AgNPs size is 2 to 7.5 nm with an average diameter of 4.5 nm (Figure 2D).

Figure 2. Characterization of AgNPs synthesized by *F. solani* and *C. aquatica*. **A.** FTIR spectrum; the boxes indicate (O-H), (N-H) and (C-H) bands of alcohol, primary amine and alkaline, respectively. C=O indicates

amide band and C-N is characteristic band of aliphatic and aromatic organic compound. **B.** XRD pattern; the numbers in the parenthesis show the face center cubic planes of AgNPs. **C.** TEM image of relatively spherical shaped AgNPs (scale bar is 50 nm). **D.** Histogram analysis of the particle size distribution.

The surface topography and morphology of AgNPs was confirmed by AFM imaging (Figure S7). The three-dimensional horizontal cross-section of the AgNPs indicates that the surface topography of the synthesized AgNPs was almost spherical in shape.

Action of AgNPs against *E. faecalis*

To investigate whether the prepared AgNPs are effective against pathogenic bacteria, local multidrug-resistance clinical pathogenic *E. faecalis* was selected as a model. It shows that nanoparticles prepared by C-FS of *F. solani* and *C. aquatica* cooperatively proved to be effective against the selected pathogen. A clear inhibition zone was observed against *E. faecalis* (Figure S8). To detect the lowest concentration that completely inhibits *E. faecalis* visible growth, the minimum inhibitory concentration (MIC) was determined (Figure 3A). The MIC of AgNPs against *E. faecalis* is 12.5% (v/v), suggesting its spectrum nature is against it. Besides, about 28% growth of *E. faecalis* was inhibited in which 9% (v/v) of AgNPs was applied. Additionally, AgNPs reduced the biofilm formation of *E. faecalis* significantly. Notably, changes in the colony and its surrounding colors on CRA in the presence of nanoparticles indicate that AgNPs have a significant role as antibiofilm activity against *E. faecalis* (Figure 3A inset). Following the biofilm results and to explore more about AgNPs mode of action, protein leakage was studied; *E. faecalis* cells were treated with 0, and 9 % (v/v) of AgNPs. Notably, protein concentration in the supernatants of treated cells was greatly increased to 7.8 mg/mL in comparison with untreated cells; about 4.7 mg/mL. Furthermore, AgNPs were investigated against antibiotics resistant genes of *E. faecalis*. As seen in Figure 3B, PCR was carried out to amplify resistant genes bla_{CTX} and bla_{TEM} in *E. faecalis*. Both genes were degraded enormously by treatment with our AgNPs formula.

Figure 3. Action of AgNPs against *E. faecalis*. **A.** Growth and biofilm inhibition. **Inset**: Five µL was taken from each well and spotted onto the LB agar (**a**) and Congo red agar plates (**b**). **B.** A representative picture of PCR amplification products using primers for bla_{TEM} and bla_{CTX} for *E. faecalis* extracted DNA. bla_{CTX} and bla_{TEM} primers (before and after treatment with AgNPs) were used. L represents the ladder (1 kb).

Discussion

Finding safe and stable AgNPs with a broad-spectrum of action is a goal of scientists, pharmacists, and physicians for more than a decade; however, developing and fabricating the right AgNPs can be challenging. The current paper is the first study, to our knowledge, investigating the use of C-FS of *F. solani* and *C. aquatica* collaboratively as biocatalysts for making AgNPs, shedding light on the metabolite-metabolite interactions between both organisms. Furthermore, the present work investigates, for the first time, the role of *C. aquatica* metabolites in AgNPs fabrication. The results indicate that

supernatants of both organisms have the potential to reduce Ag^+ to AgNPs. Notably, the solution developed a dark brown color within a few hours; therefore, it was subjected to UV-vis spectroscopy in the scan range of 300–800 nm. AgNPs absorbed light at different wavelengths and were excited due to charge density at the interface between conductor and insulator to give a respective peak at around 425 nm. A previous study reported that AgNPs in aqueous solutions show a dark brown color and displayed a wide peak at 408–411 nm (Ahmed et al. 2018). To increase the yield and stability of AgNPs, pH value, reduction time, C-FS with $AgNO_3$ solution ratio and $AgNO_3$ molarity have been studied. Adjustment of pH value can be used to control certain characteristics of the nanoparticles; however, pH varies widely based on microbes' type; pH 9.0 was found to be the optimal value for the maximum absorbance at 438 nm. The bioactive metabolites of the fungal-bacterial supernatant seem to be more stable and possess higher catalytic activity at alkaline pH. In acidic pH value, the aggregate of AgNPs was observed; whereas at pH 7.0, there was less synthesis of NPs achieved (data not shown). Birla et al. 2013 have obtained maximum nano-production from the filamentous fungus *F. oxysporum* at pH 9.0 and 11.0, with lower production at pH 7.0; in addition, the study has reported the formation of aggregates between pH 3.0 and 5.0. Moreover, Qian et al. 2013 observed that alkaline pH favored AgNPs synthesis when $AgNO_3$ was added to the filtrate of the fungus *Epicoccum nigrum*. Also, incubation of $AgNO_3$ with *Penicillium aculeatum* filtrate showed the maximal synthesis of nanoparticles at pH 8.0 with the maximum absorbance at 436 nm (Ma et al. 2017). Apparently, the intensity of the characteristic color of the AgNPs solution was directly proportional to the time of $AgNO_3$-supernatant mixture incubation. The rate of silver ion reduction was slow during the first incubation hours as indicated by the low absorbance values at the maximum absorption wavelength i.e., 453 nm. Remarkably, with an increase of the incubation time from 24 to 72 h, the absorbance intensity of the UV-vis spectra elevated and the formation of AgNPs reached the highest yield at 441 nm. An increase in the intensity of the absorbance peak with time indicates the maximum reduction of the silver ions. This difference in absorbance along with color intensity could be interpreted by the high concentration of AgNPs in relation to time. It has been reported that the time required for full reduction of the metal ions via bacterial and fungal biosynthesis of metal nanoparticles can range from 24 to 120 hours (Firdhouse and Lalitha, 2015). In the case of C-FS/silver nitrate ratio, the result of 1:2 was effective as maximum AgNPs formation occurred with an average size of about 4.5 nm in diameter which was further confirmed by the formation of the highest absorption peak and darkest brown color formation in the reaction mixture. The result was likely due to the higher amounts of metabolites in the C-FS, in particular, the enzymes that seem to be enough for performing the Ag reduction exceedingly. Moreover, the combination of metabolites in our C-FS provides a synergistic effect for stabilizing AgNPs leading to the excitation of surface plasmon vibrations evidently. The result aligned with AgNPs characterization of *Pimenta dioica* leaf extract described in literature (Rodríguez-Serrano et al. 2020). Literature also shows that 3:2cell-free filtrate/silver nitrate was effective in reducing the size of spherical AgNPs (Shahzad et al. 2019). Consistent with most of the literature where 1 mM of $AgNO_3$ is usually used for AgNPs synthesis, in this paper, although different concentrations of silver nitrate were applied, 1 mM was found to be the best. The concentration of $AgNO_3$ is a key parameter that greatly affects the synthesis process; however, very few reports studying different metal concentrations for AgNPs biogenic

synthesis are available. As the concentration of $AgNO_3$ decreased to 0.75 and 0.5 mM, the production of AgNPs decreased. In some cases, a lower concentration of $AgNO_3$ resulted in smaller nanoparticle size and an improved dispersion (Htwe et al. 2019). A concentration of 2.0 mM $AgNO_3$ triggered the maximum production of AgNPs, with the absorbance peak at 415 nm (Ma et al. 2017). Moreover, AbdelRahim et al. 2017, found that the addition of excess metal ions created very large nanoparticles with irregular morphology.

In FTIR spectroscopy measurement, the accountable bio-functional groups for the capping and stabilization of metal nanoparticles were identified. The richness of the C-FS with protein, in particular, the reductases group (data not shown in this study) plays a vital role in AgNPs formation and stabilization. The secreted metabolites by cells of fungus and bacterium have a strong affinity to bind to the AgNPs surface through free amino groups, cysteine residues, or electrostatic attraction of negatively charged carboxylate groups. Moreover, the expected enzymes and other proteins in the C-FS were not only playing roles in the reduction and capping processes, but also stabilizing AgNPs as well as protecting them from agglomeration (Hamzah et al. 2018). Intriguingly, a previous article explored the importance of *C. aquatica* in reducing the toxicity of metals and stimulating the growth of *F. solani* (Qurbani and Hamzah 2020). Here, we propose, for the first time, a coupled activity of *C. aquatica* and *F. solani* metabolites that recapitulates the reported synergistic activation for AgNPs fabrication. Consequently, more data should be necessary as it might reveal the functional principles of *C. aquatica* and *F. solani* metabolites in the synthesis process and, perhaps, shed light on the reduction mechanisms. Confirming the exact nature of the formed AgNPs, the XRD technique was conducted. As mentioned above, the XRD pattern shows some distinct peaks at 2θ values. All the reflection planes are matched and consistent with the face-centered cubic (fcc) phase of the pure crystalline silver structure's database of the Joint Committee on Powder Diffraction Standards (JCPDS). Similar results were reported using another fungal strain (Rodríguez-Serrano et al. 2020). A possible reason for the variation in the average particle size of XRD and TEM results might be due to the aggregation of particles during the drying process as well as agglomeration provoked through drying (Teulon et al. 2019).

Taking together, FE-SEM images and EDX analysis indicate the formation of nanoparticles and confirm the purity of AgNPs in which a typical absorption peak has been observed at 3keV, confirming the characteristics of metallic AgNPs. The other small peak of Au was observed as a result of gold emissions applied during sample preparation. The elemental mapping results of the biogenic AgNPs indicate the maximum distribution of the silver element in the obtained product and confirmed the purity of the silver. TEM application was used to determine the size and shape of silver NPs; in optimum conditions, AgNPs with an average size ranging from 2-7.5 nm were obtained. Rudakiya and Pawar, 2017 obtained AgNPs from *C. acidovorance* with a size of 6–53 nm having spherical, oval, and irregular shapes with a smooth surface. Also, previous findings have reported that mycosynthesized AgNPs have spherical shapes and are uniformly distributed without significant agglomeration (Ahmed et al. 2018). In atomic force microscopy, scanning the micrometric areas of the sample surface for obtaining 2D and 3D topographic images was performed. It was conducted at the nano and micro scale to analyze the structure and size of

nanoparticles, which provide considerable insight into the morphology and particle size distribution profile of the synthesized NPs.

The findings described in previous sections promote the assessment of the performance of our AgNPs, for the first time, against *E. faecalis*. As an attempt, AgNPs inhibited the growth of *E. coli, P. aeruginosa, S. aureus*, and *S. enterica* (data not shown here). Antibiotic-resistant bacteria have considerably elevated and become a worldwide problem. In previous papers, AgNPs demonstrated their remarkable bactericidal properties against both Gram-negative and Gram-positive bacteria (Velusamy et al. 2016; Du and Yi 2016). The AgNPs exhibit different bactericidal activity against various pathogenic bacteria depending on a number of factors such as size, shape, and concentration. Generally, smaller nanoparticles have greater antimicrobial effects (Lu et al. 2013; Agnihotri et al. 2014). A possible reason is that a greater surface area in contact with the cells facilitates membrane rupture and internalization. Thus, spherical AgNPs show a larger surface area to volume ratio, which leads to efficient contact with larger reaction surfaces, and this might present stronger bactericidal activity (Hong et al. 2016). Our biogenic AgNPs, based on the MIC, observed that these nanoparticles are able to inhibit the growth and the biofilm of *E. faecalis* even in very low concentrations. This might be due to the small size and spherical-shaped NPs i.e., 4.5 nm which lead to enhance the permeability of the cell membrane, formation of free radicals, and interaction with thiol groups, affect cellular signaling (data not shown), reduction of biofilm, and DNA.

The formation of biofilms dangerously limits therapy options by colonizing tissues and medical devices, such as catheters enabling the rapid dissemination of antibiotic resistance genes (Surgers et al. 2019). Similar results obtained by Singh et al. 2018 synthesized AgNPs using *Pseudomonas* sp.THG-LSI.4 showed a good inhibitory zone against various pathogenic bacteria as well as a broad-spectrum mode of action. Furthermore, the results of the biofilm inhibition indicated that the AgNPs were able to inhibit the biofilm of *E. faecalis* at a concentration of 12.5 (v/v). Our study depicts crystalline colonies-turned black on CRA as an indicator of biofilm formation. However, after treatment with 9% (v/v) AgNPs, biofilm formation is significantly reduced. Comparably, the wells of the microtiter plate are a surface for biofilm-associated cells to attach to, and as seen by the stained crystal violet, the intensity of the color is an indication of strong biofilm formation. The intensity of the crystal violet is diminished after treatment and hence, depicts the reduction of biofilm formation. These results show that a concentration of 9% AgNPs was able to inhibit and destabilize the biofilm formation of *E. faecalis*. Several mechanisms have been proposed for bactericidal activity of AgNPs. However, the exact mechanism of bactericidal activity of AgNPs remain unclear. One of the most accepted mechanisms, is that the direct contact of AgNPs with large surface areas on a bacterial cell wall could lead to produce pits resulting in the leakage of cellular contents and, eventually, cell death (Barros et al. 2018). In certain cases, small nanoparticles of size less than 10 nm particularly, can penetrate the cytoplasm and damage the respiratory chain enzyme thus, generating reactive oxygen species (ROS) such as hydrogen peroxide (H_2O_2), hydroxyl (OH–) and superoxide (O_2 –) radicals that induce oxidative stress and cause damage to proteins, reduce transcriptome and cell death (Gurunathan et al. 2018). Also, Agnihotri et al. 2014 have tried various sizes of AgNPs against *E. coli* and showed that AgNPs with sizes below 10 nm exhibited the best antibacterial

activity than larger particles. Besides, cell membranes carry a negative charge due to the presence of lipopolysaccharide, peptidoglycan and multiple groups, including carboxyl, amino and phosphate groups. Thus, positively charged silver ions can facilitate the adherence of AgNPs on bacterial membranes through electrostatic attraction between the bacteria and treated surface, causing structural change of bacterial cell wall and disruption of metabolic process which results in the degradation of cell well and, finally, cell death (Barros et al. 2018). As expected, the cell membrane of *E. faecalis* was disrupted by the action of AgNPs, and it was clearly supported by the resultant protein content in the supernatant. Level of protein leakage was higher with the cells treated with AgNPs in comparison with untreated cells. This indicates that AgNPs could increase permeability and affect membrane transport due to the serious damage of cell membrane structure.

Gel electrophoresis was performed to evaluate the action of AgNPs on the genome of *E. faecalis* (data not shown). Obviously, AgNPs reacted with DNA of *E. faecalis* since DNA seem to be reduced or degraded enormously in the case of treated cells. Additionally, the RNA was immensely decreased (data not shown). Chen et al. 2011 reported that AgNPs not only condense DNA, but also combine and coagulate with the cytoplasm of damaged bacteria, resulting in the leakage of the cytoplasmic component. Infections caused by nosocomial pathogens such as *E. faecalis* are severe in developing countries and associated with limited treatment options; therefore, some researchers are looking for new future therapeutic weapons against such strains; particularly multidrug-resistant ones; AgNPs are one of the potential therapeutic candidates. The current study has been designed to assess the mode of action against *E. faecalis*, and the results presented here are promising and warrant further investigation. Therefore, future studies aimed at assessing and producing clinically feasible sources of AgNPs for *in vivo* studies are necessary to translate these findings into clinical use. The correlation between the production of β-lactamases and the spread of resistance among isolates of Gram-positive pathogens is very high, forming serious clinical challenges (Jubeh et al. 2020). In particular, ESBLs (extended-spectrum beta-lactamases) are enzymes that deactivate β-lactam antibiotics by hydrolysis and have the ability to transfer bacterial resistance to the penicillins, first-, second-, and third-generation cephalosporins (Santos et al. 2020). ESBL-encoding genes have been categorized into three main types: $bla_{\text{CTX-M}}$, bla_{SHV} and bla_{TEM} (Ahmed et al. 2021). Our results showed that both detectable bla_{TEM} and bla_{CTX} resistant genes have deformed or damaged enormously in the case of treated cells. Additionally, the RNA smearing was greatly decreased in comparison to the untreated cells, perhaps due to the small size of synthesized AgNPs. In this context, this is the first study investigating the mode of action of AgNPs against antibiotic resistant genes in a local isolate of nosocomial *E. faecalis*, bla_{TEM}, and bla_{CTX}, and encoding the β-lactamase enzymes in the Kurdistan region of Iraq. The most notable finding of this study highly supports our hypothesis and demonstrates AgNP's ability to efficiently degrading these antibiotic-resistant genes. Simultaneously, after treatment with 9% of AgNPs, DNA and RNA of E. faecalis showed significant reduction (data not shown), while antibiotics resistant genes were completely sheared and degraded.

In this study, we found that the C-FS combination of *F. solani* and *C. aquatica* showed synergistic effects for AgNPs synthesis. The promising activity of our fabricated AgNPs against the nosocomial pathogenic *E. faecalis* suggests its potential to be used as an alternative therapeutic agent for certain medical conditions, particularly wound infection. Together, our results revealed that the C-FS of *F. solani* and *C. aquatica* has potential metabolites to reduce the silver into nanoparticles, shedding light on the interaction between both organisms. Optimization studies confirm that pH 9.0 for 72 h in 1 mM of $AgNO_3$ using 1:2 v/v (C-FS : $AgNO_3$) were the best conditions for AgNPs formation. The small size of AgNPs i.e., 2-7.5 nm and spherical shape suggests that they are stable particles. The different behavior of AgNPs against *E. faecalis* has been noticed. Protein leakage suggests that AgNPs might disrupt the cell wall and cell membrane. Reduction in genomic DNA and RNA was reported. On the other hand, this is the first study investigating AgNPs mode of action against resistance genes in *E. faecalis*. Our data call attention to the importance of investigating these resistance genes that are responsible for the spread of critical nosocomial and drug-resistant infections, where treatment options are very difficult and limited. Targeting these resistance genes could be an effective remedy in the control and surveillance of antibiotic resistance. The promising antibacterial activity enables these nanoparticles as potential bactericidal material for various environmental and biomedical applications such as water treatment, food packaging films, healthcare products, antimicrobial textiles, and wound dressings. Although the obtained AgNPs show promising antibacterial agents; however, further research is strongly recommended to investigate the safe usage of AgNP.

Abbreviations

AgNP: Silver nanoparticles; C-FS: Cell-free supernatant; XRD: X-ray diffraction; FTIR: Fourier transform infrared; FE-SEM: Field emission scanning electron; TEM: Transmission electron microscopy; AFM: Atomic force microscopy; MIC: Minimum inhibitory concentration.

Declarations

Compliance with ethical standards

The study presented here does not contain any experiments with human participants or animals performed by any of the authors.

Availability of data and materials

All data generated or analyzed during this study are available from the corresponding author upon reasonable request.

Consent for publication

Not applicable.

Competing interests

The authors declare that they have no competing interests.

Funding

The authors declare that no funding was received for conducting this study.

Authors' contributions

This work is a part of Bikhal Fattah master thesis. BF has carried out the experiments. Huner Arif is her second mentor and participated in drafting the manuscript. Haider Hamzah has designed all the experiments and drafted the paper. All authors read and approved the final manuscript.

Acknowledgments

The authors are grateful to the University of Sulaimani, Kurdistan region of Iraq for supporting the work.

References

AbdelRahim K, Mahmoud SY, Ali AM, Almaary KS, Mustafa AE, Husseiny SM (2017) Extracellular biosynthesis of silver nanoparticles using *Rhizopus stolonifer*. Saudi J Biol Sci 24(1):208-16.

Agnihotri S, Mukherji S, Mukherji S (2014) Size-controlled silver nanoparticles synthesized over the range 5–100 nm using the same protocol and their antibacterial efficacy. RSC Adv 4(8):3974-83.

Ahmed AA, Hamzah H, Maaroof M (2018) Analyzing formation of silver nanoparticles from the filamentous fungus *Fusarium oxysporum* and their antimicrobial activity. Turk J Biol 42(1):54-62.

Ahmed W, Neubauer H, Tomaso H, El Hofy FI, Monecke S, El-Tawab A, Awad A, Hotzel H (2021) Characterization of enterococci-and ESBL-producing *Escherichia coli* isolated from milk of bovides with mastitis in Egypt. Pathogens 10(2):97.

Anderson AC, Jonas D, Huber I, Karygianni L, Wölber J, Hellwig E, Arweiler N, Vach K, Wittmer A, Al-Ahmad A (2016) *Enterococcus faecalis* from food, clinical specimens, and oral sites: prevalence of virulence factors in association with biofilm formation. Front Microbiol 6:1534.

Asgary V, Shoari A, Baghbani-Arani F, Shandiz SA, Khosravy MS, Janani A, Bigdeli R, Bashar R, Cohan RA (2016) Green synthesis and evaluation of silver nanoparticles as adjuvant in rabies veterinary vaccine. Int J Nanomedicine 11:3597.

Azevedo AS, Almeida C, Melo LF, Azevedo NF (2017) Impact of polymicrobial biofilms in catheter-associated urinary tract infections. Crit Rev Microbiol 43(4):423-39.

Barros CH, Fulaz S, Stanisic D, Tasic L (2018) Biogenic nanosilver against multidrug-resistant bacteria (MDRB). J Antibiot 7(3):69.

Birla SS, Gaikwad SC, Gade AK, Rai MK (2013) Rapid synthesis of silver nanoparticles from *Fusarium oxysporum* by optimizing physicocultural conditions. Sci World J, 2013.

Blair JM, Webber MA, Baylay AJ, Ogbolu DO, Piddock LJ (2015) Molecular mechanisms of antibiotic resistance. Nat Rev Microbiol (1):42-51.

Chand K, Abro MI, Aftab U, Shah AH, Lakhan MN, Cao D, Mehdi G, Mohamed AM (2019) Green synthesis characterization and antimicrobial activity against *Staphylococcus aureus* of silver nanoparticles using extracts of neem, onion and tomato. RSC Adv 9(30):17002-15.

Chen M, Yang Z, Wu H, Pan X, Xie X, Wu C (2011) Antimicrobial activity and the mechanism of silver nanoparticle thermosensitive gel. Int J Nanomedicine 6:2873.

Dale JL, Cagnazzo J, Phan CQ, Barnes AM, Dunny GM (2015) Multiple roles for *Enterococcus faecalis* glycosyltransferases in biofilm-associated antibiotic resistance, cell envelope integrity, and conjugative transfer. Antimicrob Agents Chemother 59(7):4094-105.

Du J, Yi TH (2016) Biosynthesis of silver nanoparticles by *Variovorax guangxiensis* THG-SQL3 and their antimicrobial potential. Mater Lett 178:75-8.

Fiore E, Van Tyne D, Gilmore MS (2019) Pathogenicity of enterococci. Gram-Positive Pathogens 1:378-97.

Firdhouse MJ, Lalitha P (2015) Biosynthesis of silver nanoparticles and its applications. J Nanotechnol, 2015.

Gunasekaran T, Nigusse T, Dhanaraju MD (2011) Silver nanoparticles as real topical bullets for wound healing. J Am Coll Clin Wound Spec 3(4):82-96.

Gurunathan S, Jeong JK, Han JW, Zhang XF, Park JH, Kim JH (2015) Multidimensional effects of biologically synthesized silver nanoparticles in *Helicobacter pylori*, *Helicobacter felis*, and human lung (L132) and lung carcinoma A549 cells. Nanoscale Res Lett 10(1):1-7.

Hamedi S, Shojaosadati SA, Shokrollahzadeh S, Hashemi-Najafabadi S (2014) Extracellular biosynthesis of silver nanoparticles using a novel and non-pathogenic fungus, *Neurospora intermedia*: controlled synthesis and antibacterial activity. World J Microbiol Biotechnol 30(2):693-704.

Hamzah HM, Salah RF, Maroof MN (2018) *Fusarium mangiferae* as new cell factories for producing silver nanoparticles. J Microbiol Biotechnol 28(10):1654-63.

Hong X, Wen J, Xiong X, Hu Y (2016) Shape effect on the antibacterial activity of silver nanoparticles synthesized via a microwave-assisted method. Environ Sci Pollut Res 23(5):4489-97.

Htwe YZ, Chow WS, Suda Y, Mariatti M (2019) Effect of silver nitrate concentration on the production of silver nanoparticles by green method. Mater. Today: Proceedings 17:568-73.

Jubeh B, Breijyeh Z, Karaman R (2020) Resistance of gram-positive bacteria to current antibacterial agents and overcoming approaches. Molecules 25(12):2888.

Le Ouay B, Stellacci F (2015) Antibacterial activity of silver nanoparticles: a surface science insight. Nano today 10(3):339-54.

Lu Z, Rong K, Li J, Yang H, Chen R (2013) Size-dependent antibacterial activities of silver nanoparticles against oral anaerobic pathogenic bacteria. J Mater Sci Mater Med 24(6):1465-71.

Ma L, Su W, Liu JX, Zeng XX, Huang Z, Li W, Liu ZC, Tang JX (2017) Optimization for extracellular biosynthesis of silver nanoparticles by *Penicillium aculeatum* Su1 and their antimicrobial activity and cytotoxic effect compared with silver ions. Mater Sci Eng C 77:963-71.

Miksusanti J, Laksmi BS, Priosoeryanto BP, Syarief R, Rekso GT (2008) Mode of action Temu Kunci (*Kaempferia pandurata*) essential oil on *E. coli* K1.1 cell determined by leakage of material cell and salt tolerance assays. Hayati 15: 56–60.

Natan M, Banin E (2017) From Nano to Micro: using nanotechnology to combat microorganisms and their multidrug resistance. FEMS Microbiol Rev 41(3):302-22.

Netala VR, Bethu MS, Pushpalatha B, Baki VB, Aishwarya S, Rao JV, Tartte V (2016) Biogenesis of silver nanoparticles using endophytic fungus *Pestalotiopsis microspora* and evaluation of their antioxidant and anticancer activities. Int J Nanomedicine 11:5683.

Patel R (2005) Biofilms and antimicrobial resistance. Clin Orthop Relat Res 437:41-7.

Qian Y, Yu H, He D, Yang H, Wang W, Wan X, Wang L (2013) Biosynthesis of silver nanoparticles by the endophytic fungus *Epicoccum nigrum* and their activity against pathogenic fungi. Bioprocess Biosyst Eng 36(11):1613-9.

Qurbani K, Hamzah H (2020) Intimate communication between *Comamonas aquatica* and *Fusarium solani* in remediation of heavy metal-polluted environments. Arch Microbiol 16:1-0.

Rodríguez-Serrano C, Guzmán-Moreno J, Ángeles-Chávez C, Rodríguez-González V, Ortega-Sigala JJ, Ramírez-Santoyo RM, Vidales-Rodríguez LE (2020) Biosynthesis of silver nanoparticles by *Fusarium scirpi* and its potential as antimicrobial agent against uropathogenic *Escherichia coli* biofilms. PloS ONE 15(3):e0230275.

Rudakiya DM, Pawar K (2017) Bactericidal potential of silver nanoparticles synthesized using cell-free extract of *Comamonas acidovorans*: in vitro and in silico approaches. 3 Biotech 7(2):1-2.

Saeb A, Alshammari AS, Al-Brahim H, Al-Rubeaan KA (2014) Production of silver nanoparticles with strong and stable antimicrobial activity against highly pathogenic and multidrug resistant bacteria. Sci World J, 2014.

Santos AL, Dos Santos AP, Ito CR, Queiroz PH, de Almeida JA, de Carvalho Júnior MA, de Oliveira CZ, Avelino MA, Wastowski IJ, Gomes GP, Souza AC (2020) Profile of enterobacteria resistant to beta-lactams. J Antibiot 9(7):410.

Shahzad A, Saeed H, Iqtedar M, Hussain SZ, Kaleem A, Abdullah R, Sharif S, Naz S, Saleem F, Aihetasham A, Chaudhary A (2019) Size-controlled production of silver nanoparticles by *Aspergillus fumigatus* BTCB10: likely antibacterial and cytotoxic effects. J Nanomater, 2019.

Singh H, Du J, Singh P, Yi TH (2018) Extracellular synthesis of silver nanoparticles by *Pseudomonas* sp. THG-LS1. 4 and their antimicrobial application. J Pharm Anal 8(4):258-64.

Surgers L, Boyd A, Girard PM, Arlet G, Decré D (2019) Biofilm formation by ESBL-producing strains of *Escherichia coli* and *Klebsiella pneumoniae*. Int J Med Microbiol 309(1):13-8.

Tendolkar PM, Baghdayan AS, Gilmore MS, Shankar N (2004) Enterococcal surface protein, Esp, enhances biofilm formation by *Enterococcus faecalis*. Infect Immun 72(10):6032-9.

Teulon JM, Godon C, Chantalat L, Moriscot C, Cambedouzou J, Odorico M, Ravaux J, Podor R, Gerdil A, Habert A, Herlin-Boime N (2019) On the operational aspects of measuring nanoparticle sizes. J Nanomater 9(1):18.

Velusamy P, Kumar GV, Jeyanthi V, Das J, Pachaiappan R (2016) Bio-inspired green nanoparticles: synthesis, mechanism, and antibacterial application. Toxicol Res 32(2):95-102.

Vestby LK, Grønseth T, Simm R, Nesse LL (2020) Bacterial biofilm and its role in the pathogenesis of disease. J Antibiot 9(2):59.

Woźniak-Biel A, Bugla-Płoskońska G, Burdzy J, Korzekwa K, Ploch S, Wieliczko A (2019) Antimicrobial resistance and biofilm formation in *Enterococcus* spp. isolated from humans and turkeys in Poland. Microb Drug Resist 25(2):277-86.

Xu L, Wang YY, Huang J, Chen CY, Wang ZX, Xie H (2020) Silver nanoparticles: Synthesis, medical applications and biosafety. Theranostics 10(20):8996.

Zhang XF, Liu ZG, Shen W, Gurunathan S (2016) Silver nanoparticles: synthesis, characterization, properties, applications, and therapeutic approaches. Int J Mol Sci 17(9):1534.

Tables

Table 1 Primer sequences for detection of *bla*$_{CTX}$ and *bla*$_{TEM}$

Primer name	Primer sequence (5’-3’)	Amplicon size (~ bp)	Antibiotic resistant
blaTEM_F	GATCCTTGAGAGTTTTCGCC	530	Ampicillin
blaTEM_R	GCAGAAGTGGTCCTGCAACT		
blaCTX_F	AGACTGGGTGTGGCATTGAT	600	Cefotaxime
blaCTX_R	CCAGGAAGCAGGCAGTCC		

*In the following primers, F denotes forward and R denotes reverse.

Figures

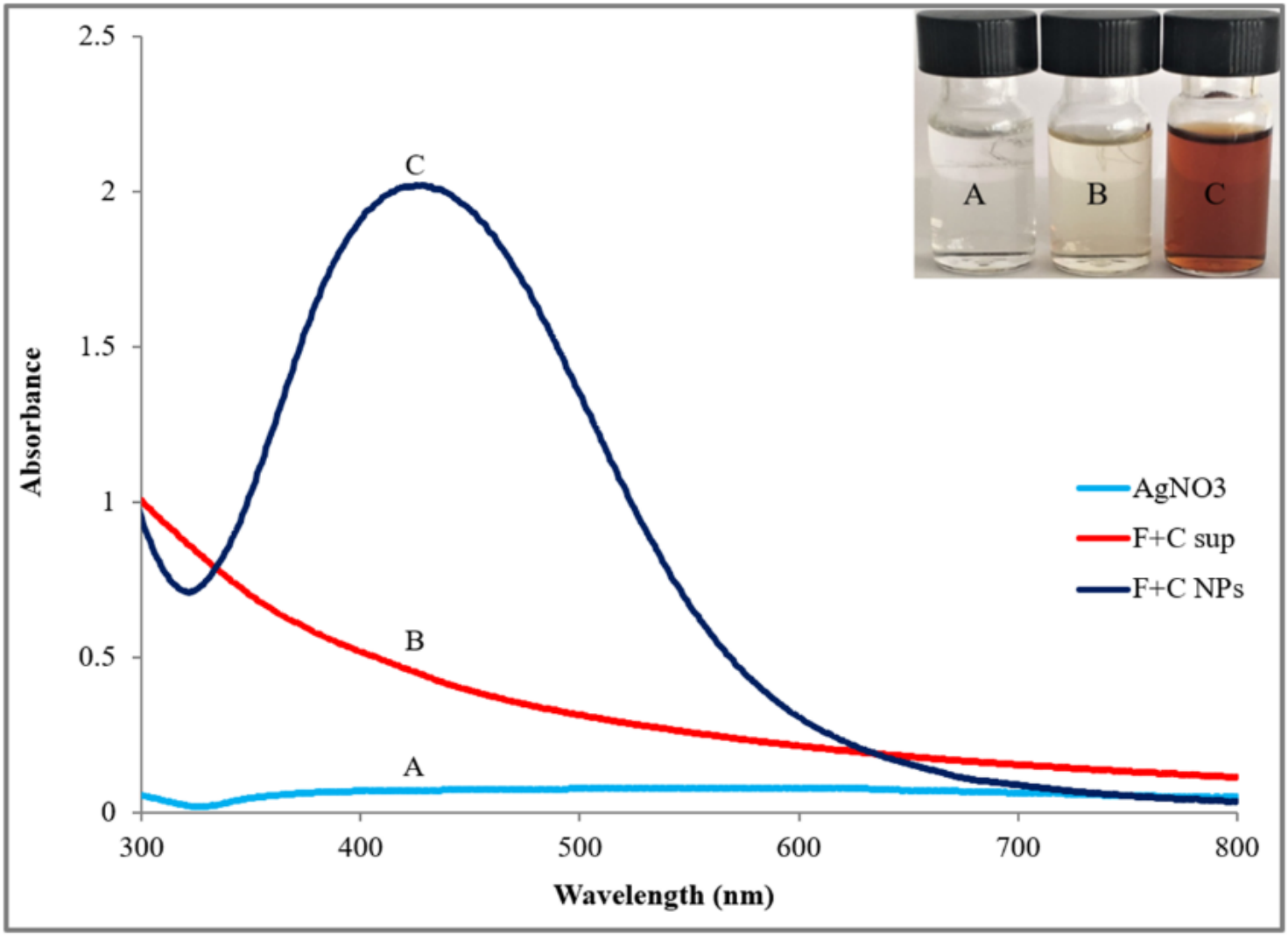

Figure 1

UV–visible spectrum of optimal conditions of AgNPs production. Inset: A. AgNO3 solution without supernatant. B. C-FS. C. C-FS and AgNO3 solution.

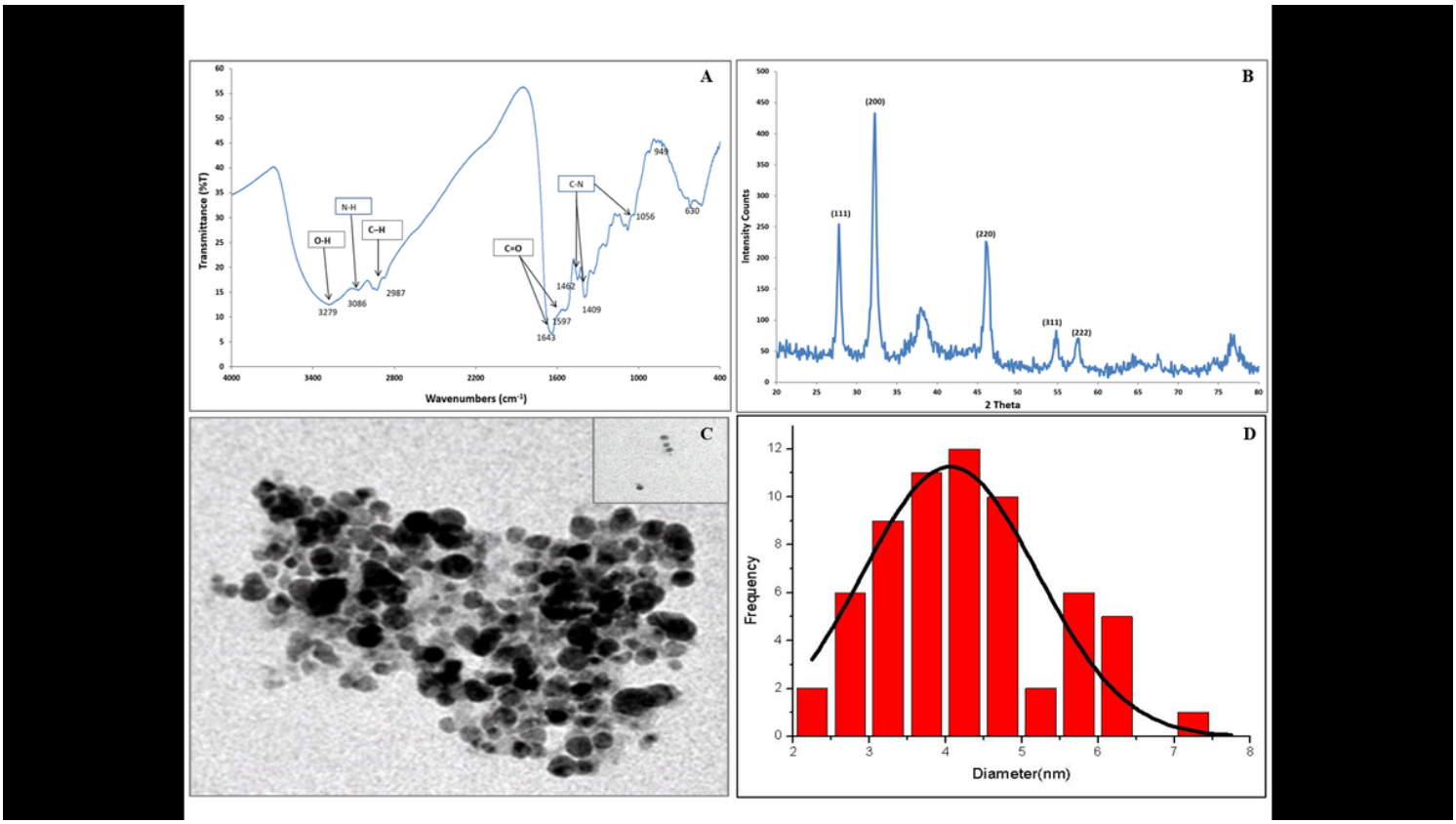

Figure 2

Characterization of AgNPs synthesized by F. solani and C. aquatica. A. FTIR spectrum; the boxes indicate (O-H), (N-H) and (C-H) bands of alcohol, primary amine and alkaline, respectively. C=O indicates amide band and C-N is characteristic band of aliphatic and aromatic organic compound. B. XRD pattern; the numbers in the parenthesis show the face center cubic planes of AgNPs. C. TEM image of relatively spherical shaped AgNPs (scale bar is 50 nm). D. Histogram analysis of the particle size distribution.

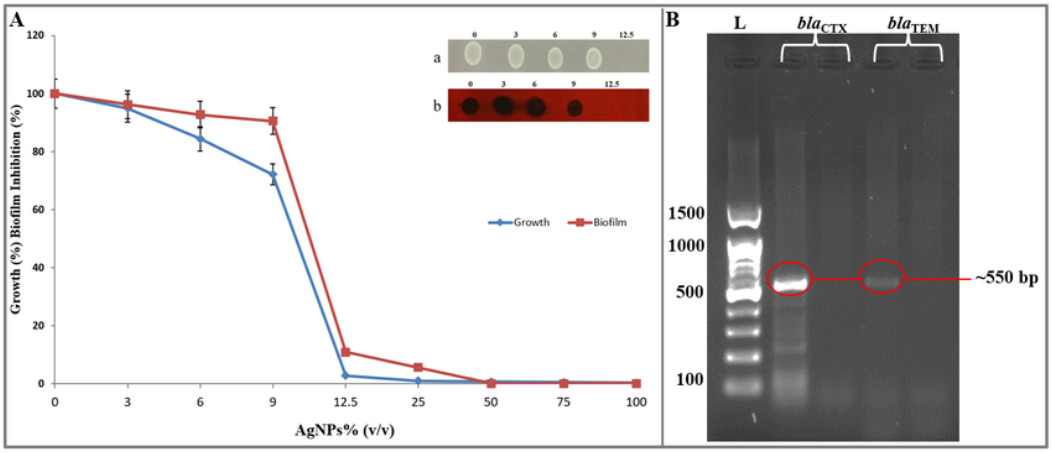

Figure 3

Action of AgNPs against E. faecalis. A. Growth and biofilm inhibition. Inset: Five µL was taken from each well and spotted onto the LB agar (a) and Congo red agar plates (b). B. A representative picture of PCR amplification products using primers for blaTEM and blaCTX for E. faecalis extracted DNA. blaCTX and blaTEM primers (before and after treatment with AgNPs) were used. L represents the ladder (1 kb).

Supplementary Files

This is a list of supplementary files associated with this preprint. Click to download.

- FigureS1.docx
- FigureS2.docx
- FigureS3.docx
- FigureS4.docx
- FigureS5.docx
- FigureS6.docx
- FigureS7.docx
- FigureS8.docx